

# Examination of the Details of 2D Vorticity Generation Around the Airfoil During Starting and Stopping Phases

Alwin Wang  
Supervised By: Hugh Blackburn

[The format of this research paper is different from standard template after consultation with my supervisor]

## Abstract

This paper presents a numerical study of vorticity generation around a 2D airfoil during the starting and stopping phases of motion. The study focuses on a single NACA0012 airfoil of unit chord at  $4^\circ$  angle of attack where the two-dimensional Navier-Stokes equations are solved using a spectral element DNS code. Peaks in the boundary vorticity flux on trailing edge surface support recent arguments of how the Kutta condition is established. The peaks in lift force during the starting and stopping phases appear to be well-explained by thin airfoil theory for non-uniform motion.

## 1 Introduction

Around 1930, Prandtl, Tietjens and Müller recorded the motion of fine particles around an airfoil in the starting and stopping phases of motion to observe transient, unsteady flows[9]. The original recordings have been analysed using modern particle image velocimetry (PIV) by Willert and Kompenhans [14] and the phenomena of starting and stopping vortices still remains of interest.

Vincent and Blackburn [12] showed the formation of these vortices by performing a direct numerical simulation (DNS) of transient flow over a NACA0012 airfoil at  $Re = 10,000$  and  $\alpha = 4^\circ$  while Agromayo, Rúa and Kristoffersen [1] investigated a NACA4612 at  $Re = 1,000$  and  $\alpha = 16^\circ$  using OpenFOAM. Both studies determined coefficients of lift and drag during the starting and stopping phases and verified Kelvin's and Stoke's theorems, shown in equation (1), for vorticity around various contours. This paper expands on these studies by considering the vorticity generation mechanisms and exploring the physical phenomena behind vortices generated during

the starting and stopping phases.

$$\Gamma = \oint_C \vec{V} \cdot d\vec{l} = \iint_S \vec{\nabla} \times \vec{v} \cdot dS = \iint_S \vec{\omega} \cdot d\vec{S} \quad (1)$$

It is recognised that the sources of vorticity must occur at the boundary of the fluid regions and for the starting and stopping phases of motion. Morton [10] outlines two production mechanisms for vorticity: tangential pressure gradients from the fluid side, and the acceleration of the surface from the wall side, shown in equation (2). These contributions were investigated by Blackburn and Henderson [3] for vortex shedding of oscillating cylinders and it was noted that the pressure-gradient generation mechanism could override the surface-acceleration generation mechanism and vice versa.

$$-\nu \left( \frac{\partial \vec{\omega}}{\partial z} \right)_0 = -\frac{1}{\rho} [(\vec{n} \times \nabla) \vec{p}]_0 - \vec{n} \times \frac{d\vec{V}}{dt} \quad (2)$$

Zhu et al. [15] investigated the causal mechanisms for airfoil circulation using vorticity creation theory based on Lighthill's relations [6], shown in equation (3), instead of boundary-layer theory. Additionally, the realisation of the Kutta condition and creation of starting vortex were determined through a complex chain of processes which were also explained by considering boundary vorticity flux,  $\sigma$ , equation (3).

$$\frac{1}{\rho} = \frac{\partial p}{\partial s} = \nu \frac{\partial \omega}{\partial n} \equiv \sigma \quad (3)$$

Another point of interest identified by Vincent and Blackburn [12] and Agromayo, Rúa and Kristoffersen [1] was the large value of lift during the starting (accelerating) phase. Kármán and Sears [5] attributed this to unsteady flows over airfoils which was later extended by Liu et al. [8] and Limacher, Morton and Wood [7]. After the starting phase, when the airfoil had attained a uniform velocity, it was also observed the lift force would asymptote to a steady-state value.

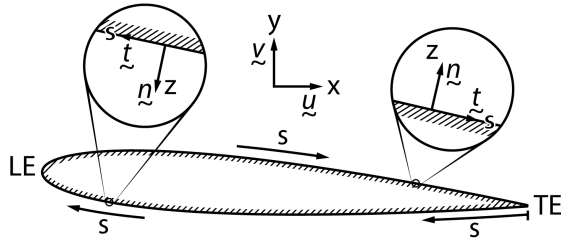


Figure 1: Coordinate system used in this analysis

An explanation for this was also provided by Kármán and Sears [5] due to a “lift deficiency” term from the effect of wake vorticity sheet generated during acceleration. This behaviour was also detailed in Saffman explaining latency in lift production known as the “Wagner effect” [11, 13].

When the no slip condition holds, Limacher, Morton and Wood [7] state that  $\vec{P}_i + \vec{P}_\Phi = 0$  which leads to their second, no slip formulation for vortex impulse where  $\vec{F} = -\rho \frac{d\vec{P}}{dt}$ . This can be used to determine the lift and drag forces and may explain the high values observed

$$\vec{P} = \vec{P}_v + \vec{P}_b = \frac{1}{N-1} \int_V (\vec{x} \times \vec{\omega}) dV - \vec{u}_c V_b \quad (4)$$

Both of these effects will also be investigated in this study of vorticity production as the vorticity is not contained to a thin region.

## 2 Numerical Method

### 2.1 Governing Equations and Numerical Approach

Simulation was carried out using the Semtex code [4] which is a spectral element-Fourier DNS code. The governing equations solved were the non-dimensionalised Navier-Stokes equations in the moving reference frame fixed to the airfoil,

$$\nabla \cdot \vec{u} = 0 \quad (5)$$

$$\frac{\partial \vec{u}}{\partial t} + \vec{u} \cdot \nabla \vec{u} = -\nabla \vec{P} + \frac{1}{Re} \nabla^2 \vec{u} - \vec{a} \quad (6)$$

where  $\vec{P} = \frac{\rho}{\rho} \vec{P}$  and  $\vec{a}$  is the acceleration of the reference frame. The boundary conditions at prescribed velocity boundaries are set as  $\vec{u} = -V(t)$  where  $V(t)$  is the velocity of the reference frame such that  $a = V'(t)$ .

For motion of a two-dimensional plane boundary moving in its own plane with velocity  $\vec{V} = (V(t), 0)$ ,

the diffusive flux density (flow per unit length per unit time) of positive vorticity outwards from the wall is given as:

$$-\sigma \equiv -\nu \frac{\partial \vec{\omega}}{\partial z} \Big|_{z=0} = -\vec{n} \times (\nabla \vec{P} + \vec{a}) \quad (7)$$

where  $\vec{\omega}$  is the vorticity,  $\vec{n}$  is the unit wall-normal vector,  $z$  is the distance normal to the surface and  $\vec{a}$  is the local wall acceleration [10]. The term boundary vorticity flux (BVF),  $\sigma$ , has been introduced based on Zhu et al. [15].

It is assumed that a local section of airfoil can be modelled as an infinite plane with negligible curvature and the acceleration of the plane is given by  $\vec{t} \cdot \vec{a}$  where  $\vec{t}$  is a unit tangent vector as shown in figure 1. Thus, the vorticity production around the airfoil is given by equation 8a in vector form and equation 8b for a particular point on the airfoil.

$$-\nu \vec{n} \cdot \nabla \vec{\omega} = -\vec{n} \times \nabla \vec{P} - \vec{t} \cdot \vec{a} \quad (8a)$$

$$-\nu \frac{\partial \omega}{\partial z} = -\frac{1}{\rho} \frac{\partial p}{\partial s} - \frac{dV}{dt} \quad (8b)$$

It is clear that the convergence of second derivatives for  $u$  and  $v$  are required to accurately determine  $\nabla \vec{\omega}$ .

The acceleration profile for the airfoil was chosen to be the same as Vincent and Blackburn [12] which represents non-impulsively started flow to unity free-stream velocity (figure 2). In Saffman’s [11] the explanation of the “Wagner effect” [13], it is noted that the initial lift is one-half of the final steady-state lift after a time  $O(c/v)$ . As such, a period of 0.8s of uniform flow between the starting and stopping phases allows the convergence of lift to be investigated.

### 2.2 Grid and Time Step Refinement

To determine an appropriate choice for the order of the tensor-product GLL shape functions used in each spectral element, tests were conducted at  $t = 0.15$ s which corresponded to the maximum forwards (negative) acceleration of the airfoil. A  $p$ -Convergence test where  $p$  is the order of the tensor-product was performed. Values of  $p$  between 3 and 19 were used and their results compared to  $p = 20$ . The result is shown in figure 4. A value of  $p = 10$  was chosen .

The final spectral element mesh used had 989 conforming quadrilateral spectral elements as shown in figure (5). Local mesh refinement was concentrated near the surface of the airfoil to resolve the boundary layer. 8<sup>th</sup>-order tensor-product nodal basis functions

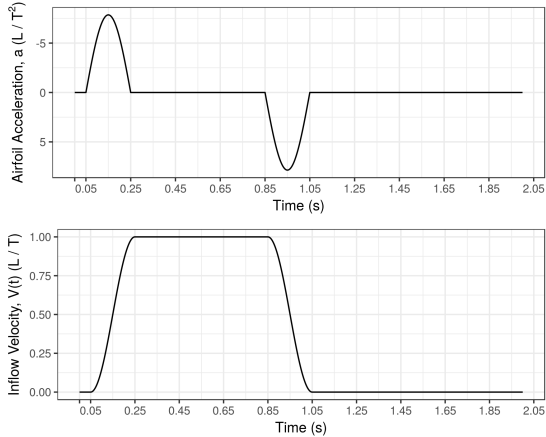


Figure 2: Airfoil during the starting and stopping phases. Note that the definition of  $x$  is consistent with the solution domain of accelerating reference frame.

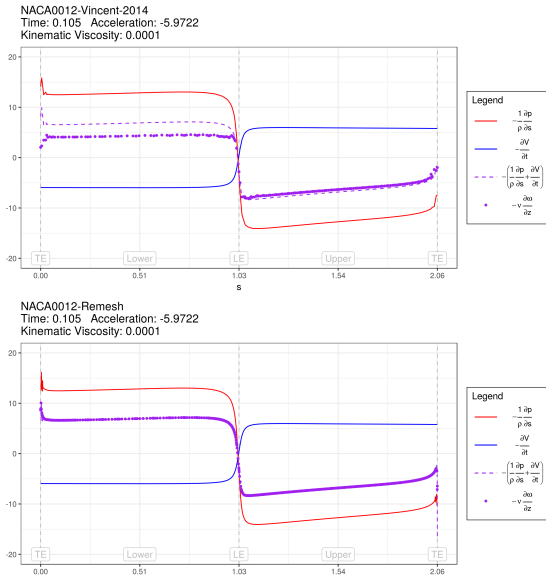


Figure 3: Comparison in ability to resolve equation (8b) for vorticity generation. The dashed purple line represents the RHS of the equation and the purple dots represent the LHS.

Top: Vincent and Blackburn [12] mesh. Bottom: Refined mesh

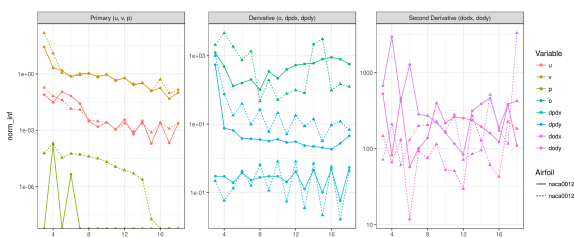


Figure 4:  $p$ -Convergence study results

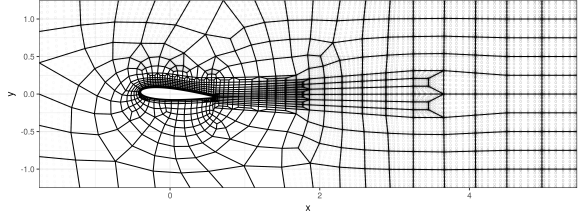


Figure 5: Spectral Element Mesh

were used in each element, giving a total of 63,296 independent mesh nodes.

### 2.3 Unsteady Thin-Airfoil Theory

According to classic thin airfoil theory provided in Anderson [2] the vortex sheet strength of an airfoil,  $\gamma(\xi)$ , can be determined as

$$\frac{1}{2\pi} \int_{-1}^1 \frac{\gamma(\xi)}{x - \xi} = V_\infty \left( \alpha - \frac{dz}{dx} \right) \quad (9)$$

where the terminals have been adjusted to match the definition provided in [5] and  $\frac{dz}{dx} = 0$  in this analysis as the NACA0012 is a symmetric airfoil. This can be applied to Kármán and Sears [5] derivation for the lift of a thin airfoil in non-uniform motion:

$$L = \underbrace{\rho V_\infty \Gamma_0}_{\text{Quasi-Steady}} - \underbrace{\rho \frac{d}{dt} \int_{-1}^1 \gamma_0(x) x \, dx}_{\text{Apparent Mass}} - \underbrace{\rho V_\infty \int_1^\infty \gamma(\varepsilon) \frac{d\varepsilon}{\sqrt{\varepsilon^2 - 1}}}_{\text{Wake Effect}} \quad (10)$$

where  $\gamma_0(x)$  and  $\Gamma_0$  are the vortex sheet strength and circulation respectively, calculated from thin airfoil theory, equation (??).  $\gamma(\varepsilon)$  is the vorticity of the wake assumed to be on the airfoil plane a distance  $\varepsilon$  from the mid chord ( $x = 0$ ).

While Kármán and Sears [5] present a solution for the wake effect term, from PIV by Willert and Kompenhans [14] it is clear the assumption of the wake remaining in the same plane as the airfoil does not hold as wake vortex sheet rolls up to form the starting vortex. Thus, only the first two terms, quasi-steady state,  $L_0$ , and apparent mass,  $L_1$ , are investigated.

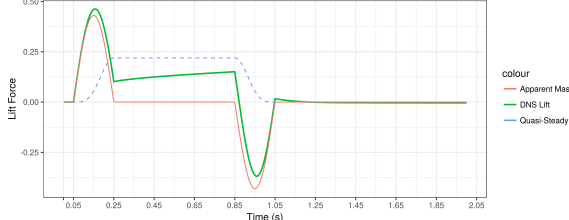


Figure 6: Unsteady lift estimation using equation (10)

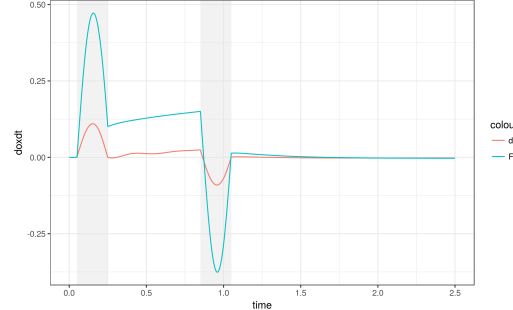


Figure 8: Lift versus time  $0 \leq t \leq 2.5$  for  $Re = 1,000$

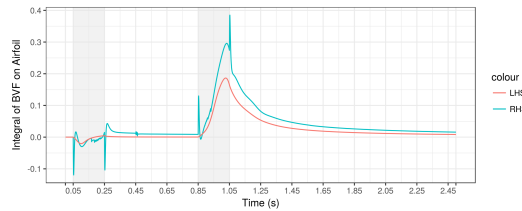


Figure 7: Integral of BVF versus time  $0 \leq t \leq 2.5$  for  $Re = 10,000$

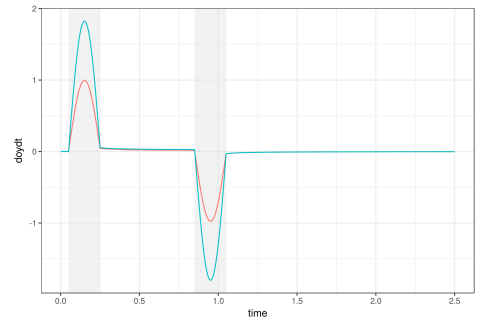


Figure 9: Drag versus time  $0 \leq t \leq 2.5$  for  $Re = 10,000$

### 3 Results and Discussion

#### 3.1 Starting Vortex and Establishing the Kutta Condition

In figure 10 it can be seen that in second half of the starting phase,  $t \in [0.15, 0.25]$  s, the vorticity on the upper and lower surfaces are not equal. When  $t \in [0.25, 0.85]$  s it can be seen that the vorticity on the upper and lower surfaces approach each other and, given sufficient time, will be equal at the trailing edge and satisfy the Kutta condition. In comparison, it is noted that the leading edge vorticity appears to have reached a steady-state much faster.

When analysing the key stages in establishing the Kutta condition, Zhu [15] recognised the importance of sharp BVF peaks on both sides of the trailing edge as shown in figure 11. These peaks are also present in this non-impulsively-started flow which supports this argument.

It is noticed that the leading edge also has sharp BVF peaks that vary with time during the stopping phase,  $t \in [0.85, 1.05]$  s in a similar fashion to the trailing edge. This could contribute to the formation of leading edge stopping vortices observed by Vincent and Blackburn [12].

#### 3.2 Unsteady Thin-Airfoil Theory

Figure 10 compares the quasi-steady and apparent mass terms of equation (10) with the result from DNS. Immediately it is clear that apparent mass is the major contributor to the large lift force during the starting and stopping phases. At the end of the stopping phase, the DNS lift is approximately one half of the quasi-steady lift which is in agreement with Saffman's statement that the initial lift is one-half of the final steady-state lift [11]. Even without the wake-effect term, it appears that equation (10) well describes the phenomena observed.

#### 3.3 Vortex Impulse

It can be seen from Figure 8 that the vortex impulse for lift,  $\frac{d}{dt} \int_V \omega \times y dV$ , and vortex impulse for drag,  $\frac{d}{dt} \int_V \omega \times x dV$ , so help explain the peaks in the lift and drag values observed. The remaining value can be attributed to the added mass force outlined by Limacher, Morton and Wood [7] in combination with the result from unsteady thin-airfoil theory.

## 4 Conclusions

This paper further develops the study of vorticity generation mechanisms by applying them to the starting and stopping phases of airfoil motion. The results corroborate phenomena observed by other authors in a non-impulsively-started flow. Unsteady thin airfoil theory was also applied to explain the vertical forces observed during the starting and stopping phases.

## References

- [1] Agromayor, R., Rúa, J. and Kristoffersen, R., Simulation of Starting and Stopping Vortices of an Airfoil, in *Proceedings of the 58th Conference on Simulation and Modelling (SIMS 58) Reykjavik, Iceland, September 25th – 27th, 2017*, Linkoping University Electronic Press, 2017.
- [2] Anderson, J., *Fundamentals of Aerodynamics*, Aeronautical and Aerospace Engineering Series, McGraw-Hill, 2010, 5 edition.
- [3] Blackburn, H. M. and Henderson, R. D., A study of two-dimensional flow past an oscillating cylinder, *Journal of Fluid Mechanics*, **385**, 1999, 255–286.
- [4] Blackburn, H. M. and Sherwin, S. J., Formulation of a Galerkin spectral element–Fourier method for three-dimensional incompressible flows in cylindrical geometries, *Journal of Computational Physics*, **197**, 2004, 759–778.
- [5] Kármán, T. V. and Sears, W. R., Airfoil Theory for Non-Uniform Motion, *Journal of the Aeronautical Sciences*, **5**, 1938, 379–390.
- [6] Lighthill, J., *An Informal Introduction to Theoretical Fluid Mechanics*, Oxford University Press, 1986.
- [7] Limacher, E., Morton, C. and Wood, D., Generalized derivation of the added-mass and circulatory forces for viscous flows, *Physical Review Fluids*, **3**.
- [8] Liu, T., Wang, S., Zhang, X. and He, G., Unsteady Thin-Airfoil Theory Revisited: Application of a Simple Lift Formula, *AIAA Journal*, **53**, 2015, 1492–1502.
- [9] Ludwig Prandtl, O. K. G. T., *Applied hydro- and aeromechanics*, New York ; London : McGraw-Hill Book Company, inc, 1934, 1st ed edition, plates: p. [277]-306.
- [10] Morton, B. R., The generation and decay of vorticity, *Geophysical & Astrophysical Fluid Dynamics*, **28**, 1984, 277–308.
- [11] Saffman, P. G., *Vortex Dynamics (Cambridge Monographs on Mechanics)*, Cambridge University Press, 1993.
- [12] Vincent, M. and Blackburn, H. M., Simulation of starting/stopping vortices for a lifting aerofoil, in *Proceedings of the 19th Australasian Fluid Mechanics Conference (AFMC)*, editors H. Chowdhury and F. Alam, RMIT University, 2014, 1–4, 1–4.
- [13] Wagner, H., Über die Entstehung des dynamischen Auftriebes von Tragflügeln, *ZAMM - Zeitschrift für Angewandte Mathematik und Mechanik*, **5**, 1925, 17–35.
- [14] Willert, C. and Kompenhans, J., PIV Analysis of Ludwig Prandtl's Historic Flow Visualization Films, *arXiv preprint*.
- [15] Zhu, J. Y., Liu, T. S., Liu, L. Q., Zou, S. F. and Wu, J. Z., Causal mechanisms in airfoil-circulation formation, *Physics of Fluids*, **27**, 2015, 123601.

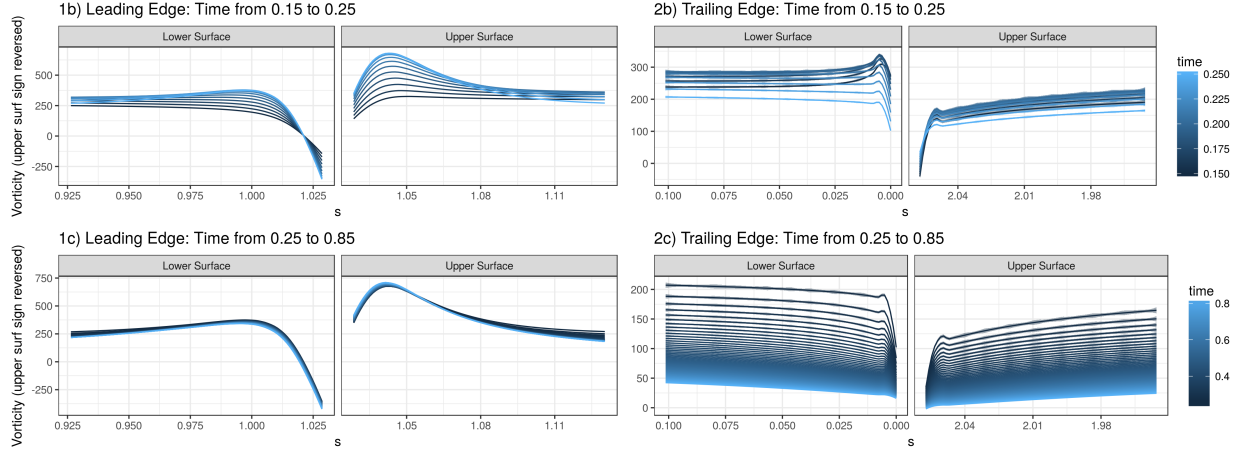


Figure 10: Vorticity on the airfoil surface for the first 10% of the chord and last 10% of the chord

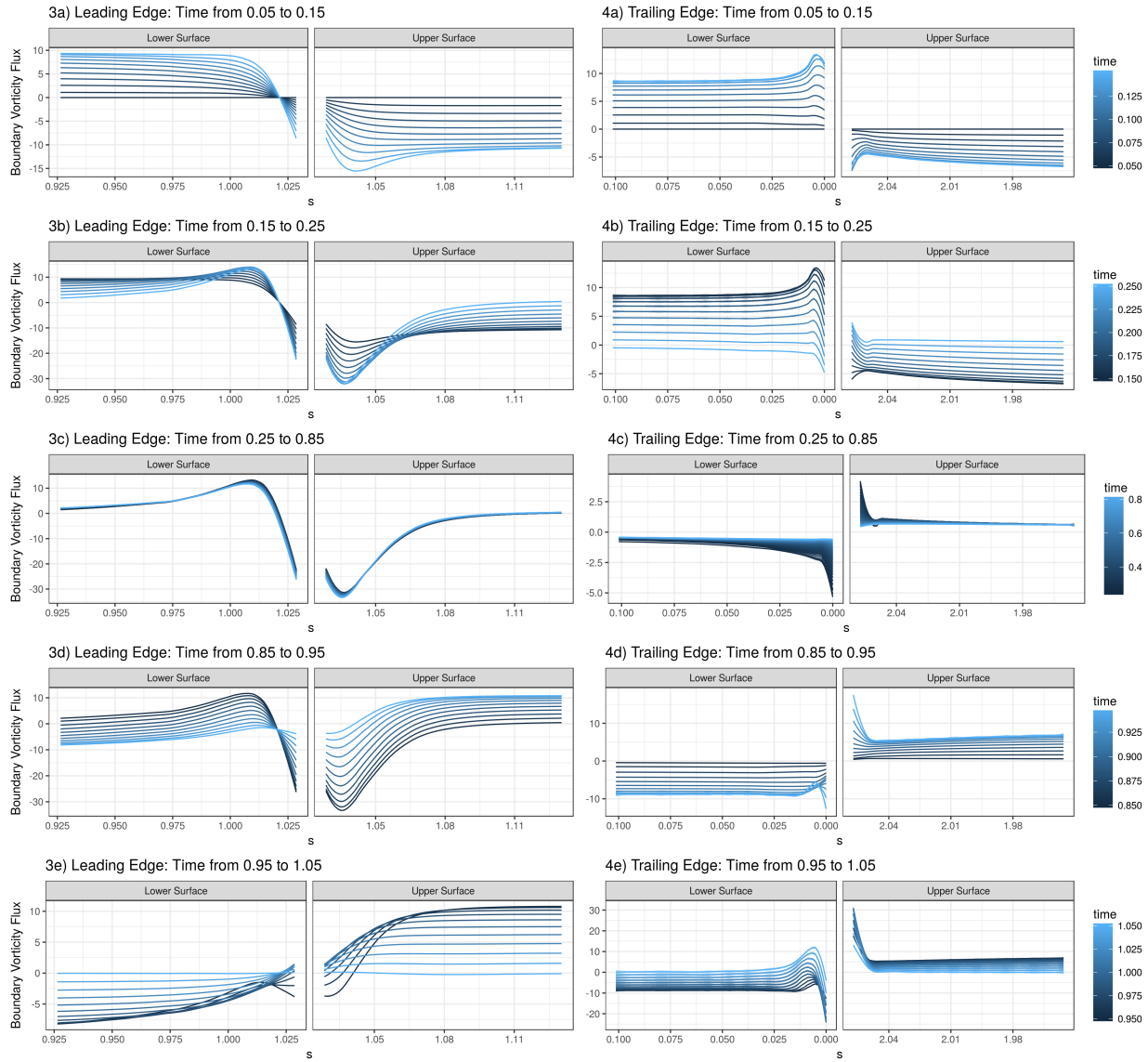


Figure 11: Vorticity production on the airfoil surface for the first 10% of the chord and last 10% of the chord